A Resonant Graphene NEMS Vibrometer

Downloaded from: https://research.chalmers.se, 2022-11-19 13:34 UTC

Citation for the original published paper (version of record):
Moreno-Garcia, D., Fan, X., Smith, A. et al (2022). A Resonant Graphene NEMS Vibrometer. Small, In Press. http://dx.doi.org/10.1002/smll.202201816

N.B. When citing this work, cite the original published paper.

research.chalmers.se offers the possibility of retrieving research publications produced at Chalmers University of Technology.
It covers all kind of research output: articles, dissertations, conference papers, reports etc. since 2004.
research.chalmers.se is administrated and maintained by Chalmers Library

(article starts on next page)

NANO · MICRO small
www.small-journal.com

A Resonant Graphene NEMS Vibrometer

Daniel Moreno-Garcia, Xuge Fan, Anderson D. Smith, Max C. Lemme, Vincenzo Messina, Cristina Martin-Olmos, Frank Niklaus, and Luis Guillermo Villanueva**

Measuring vibrations is essential to ensuring building structural safety and machine stability. Predictive maintenance is a central internet of things (IoT) application within the new industrial revolution, where sustainability and performance increase over time are going to be paramount. To reduce the footprint and cost of vibration sensors while improving their performance, new sensor concepts are needed. Here, double-layer graphene membranes are utilized with a suspended silicon proof demonstrating their operation as resonant vibration sensors that show outstanding performance for a given footprint and proof mass. The unveiled sensing effect is based on resonant transduction and has important implications for experimental studies involving thin nano and micro mechanical resonators that are excited by an external shaker.

1. Introduction

Vibrations are typically measured by accelerometers, which are present in many commodity products such as mobile phones.[1–3] However, since accelerometers are based on inertial forces, they suffer from an inherent drawback in terms of footprint: a larger mass provides a larger inertial force, and more compliant springs provide a larger deflection. With typical technological solutions, compliance is attained by increasing the springs length, thus increasing the footprint of the accelerometer. One possible solution to bypass this limitation is to use extremely compliant springs that allow reducing lateral device dimensions, i.e., using extremely thin materials like graphene. We introduced this concept recently and we have demonstrated its capabilities for use as a miniaturized accelerometer,[4–6] where one observes the deflection of the mass which is proportional to the acceleration input. Indeed, although this is the standard way of operation for most accelerometers, it comes at the cost of a direct trade-off between the responsivity and bandwidth of the sensor. As an alternative, it is possible to bypass this trade-off by utilizing accelerometers that transduce the vibrations into shifts of the device resonance frequency.

Micro- and Nano-electromechanical (MEMS and NEMS) resonant sensors have been utilized in the past 2–3 decades for several applications.[7] Resonant MEMS accelerometers have been thoroughly explored, but their typical dimensions are relatively large,[8–12] thus rendering them less interesting for internet of things (IoT)[13] and predictive maintenance applications, which require miniaturized sensors and actuators. In this work, we present the use of graphene-based accelerometers in resonant mode.

Graphene-based resonant NEMS[14–17] have raised a lot of interest in the past decade due to the outstanding mechanical properties of graphene,[18] as well as the minimal dimensions that can be attained.[19] Indeed, the ultimate thinness of graphene (single-layer thickness of 0.355 nm), together with its mechanical robustness (fracture strain of up to 30%), have motivated the study of graphene NEMS resonators, ever since the first demonstration.[20] Outstanding responsivities have been shown with respect to charges, voltage,[11,21] temperature,[22,23] mass,[22] and strain.[24]

Graphene resonators have been suggested for use as accelerometers in purely theoretical works,[25–29] but no resonant graphene accelerometer has been experimentally demonstrated to date. The main reason is the low mass of graphene devices,

D. Moreno-Garcia, V. Messina, L. G. Villanueva
Advanced NEMS Group
École Polytechnique Féderale de Lausanne (EPFL)
Lausanne 1015, Switzerland
E-mail: guillermo.villanueva@epfl.ch

X. Fan, F. Niklaus
Division of Micro and Nanosystems
School of Electrical Engineering and Computer Science
KTH Royal Institute of Technology
Stockholm SE-10044, Sweden
E-mail: frank@kth.se

X. Fan
Adv. Research Institute of Multidisciplinary Sciences
Beijing Institute of Technology
Beijing 100081, China

A. D. Smith
Department of Electrical Engineering
Chalmers University of Technology
Gothenburg 41296, Sweden

M. C. Lemme
Chair of Electronic Devices
Faculty of Electrical Engineering and Information Tech
RWTH Aachen University
52074 Aachen, Germany

C. Martin-Olmos
Swiss Integrative Center for Human Health (SICHH)
Fribourg 1700, Switzerland

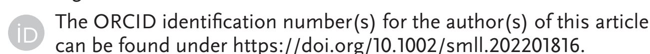
The ORCID identification number(s) for the author(s) of this article can be found under https://doi.org/10.1002/smll.202201816.

© 2022 The Authors. Small published by Wiley-VCH GmbH. This is an open access article under the terms of the Creative Commons Attribution-NonCommercial License, which permits use, distribution and reproduction in any medium, provided the original work is properly cited and is not used for commercial purposes.

DOI: 10.1002/smll.202201816

which renders them unfavorable for acceleration sensing. But we overcome this, as introduced above, by the combination of graphene and an attached silicon (Si) mass within the device.

2. Results

Our NEMS accelerometer consists of a fully clamped graphene membrane with a large attached Si proof mass (from $20 \times 20 \times 16.4$ to $50 \times 50 \times 16.4$ μm^3) (**Figure 1**a). The SEM image of a fabricated device is shown in Figure 1b. A priori, the principle of operation is that external accelerations forces act on the proof mass creating a deflection of the graphene membranes. The displacement of the suspended graphene membrane results in stress that builds up in the membrane, thereby causing a change in the resonance frequency of the spring-mass system (Figure 1c–e).

We developed a heuristic model of the devices (Section S1, Supporting Information), starting from a general solution for the load-deflection relation,[30] containing 3 terms: one linear term proportional to the Young's modulus (flexural rigidity term), a second linear term proportional to the intrinsic tension within the graphene film (tension term), and a third term, which is nonlinear, that depends on the Young's modulus and the mass displacement to the cube (Duffing term). This latter term, the nonlinear one, shows that a tension induced in the graphene membrane causes a resonance frequency shift due to a certain applied acceleration. Importantly, this frequency shift is proportional to the square of the mass displacement but, since motion happens around a DC term of acceleration

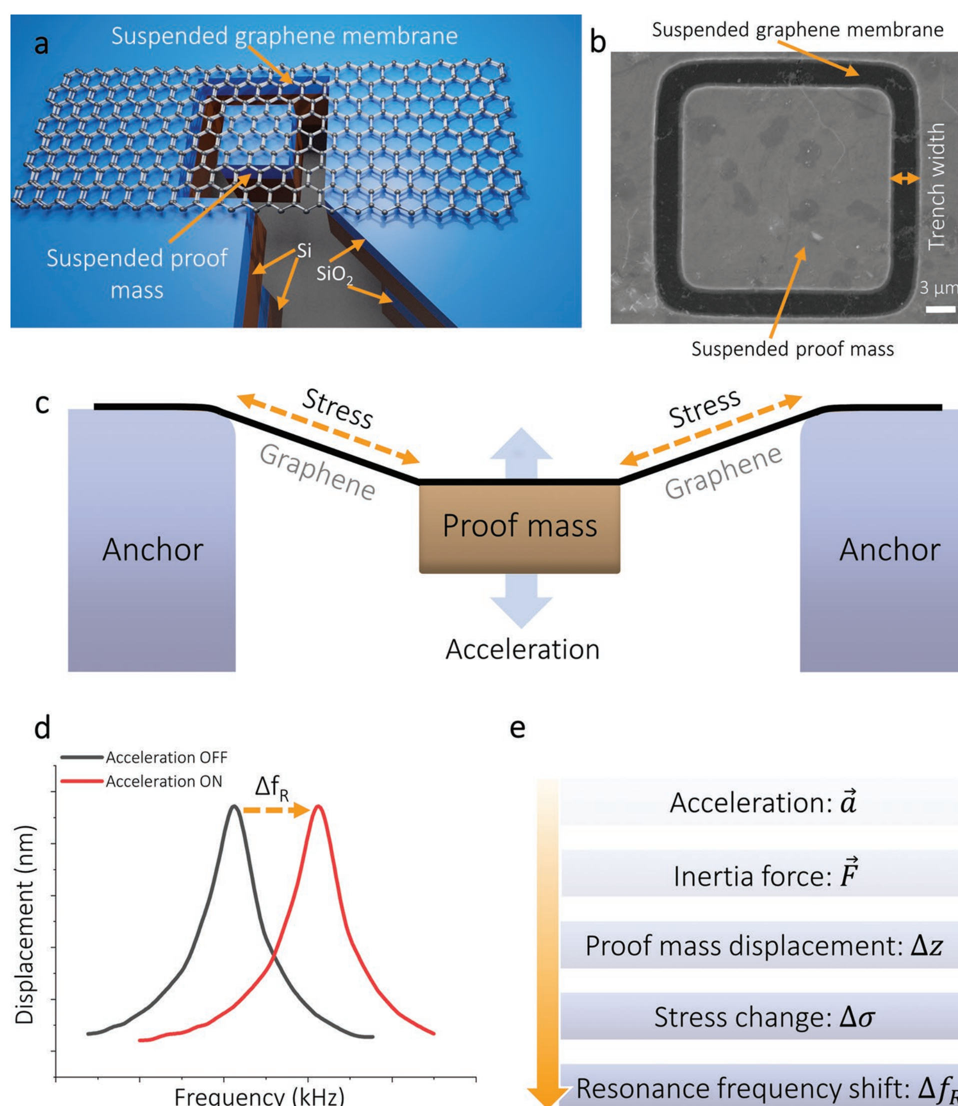

Figure 1. Sensing principle. a) 3D schematic of the resonant accelerometer: a silicon proof mass is suspended by a graphene membrane across a narrow trench. The substrate is composed of an SOI wafer with a thermally oxidized surface. Fabrication is described elsewhere.[4–6] b) Top SEM image of the device (trench width: 3 µm, mass volume: $20 \times 20 \times 16.4$ μm^3). c–e) Schematic of the operation principle: the external acceleration ($\bar{a}$) induces an inertial force ($\bar{F}$) which causes a displacement (δz) of the silicon proof mass which, in turn, yields additional tensile stress ($\delta\sigma$) on the graphene membrane, causing the resonance frequency of the system (membrane-mass) to shift δf, as illustrated in (d) and specified in (e).

 © 2022 The Authors. Small published by Wiley-VCH GmbH

(the Earth's gravity), the response to vibrations is linearized and thus happens at the same frequency as the external load. We used finite element method (FEM) simulations (Section S2, Supporting Information) to verify the quality of the model and to determine the values for the proportionality constants. The model predicts a larger responsivity when the built-in stress in the membrane is smaller.

For the device fabrication, we followed the fabrication route described in previous studies.[4–6] Details of the device fabrication can be found in Section S3 in the Supporting Information. The Si proof masses of all fabricated devices are 16.4 µm thick and have a square shape with side lengths ranging from 20 to 50 µm. The trench width of all measured devices is 3 µm.

We performed atomic force microscope (AFM) measurements to observe the residues on the graphene surface and to characterize the DC spring constant of the membranes with attached Si proof mass, concluding that in some devices the membrane tension was not uniform (Section S4, Supporting Information). The nonuniformity in the stress makes that the mode shape is never perfectly symmetric. Unfortunately, making an accurate estimation of this nonuniformity is rather difficult. Therefore, we chose to use an equivalent stress-based model, acknowledging that this could bring some dispersion for similar values of equivalent stress in our structures.

We bring the graphene-based resonators into resonant motion and track their frequency over time, as explained in Sections 5 and 6 in the Supporting Information. We then test the sensors against a harmonic excitation via external accelerations. Results in **Figure 2** are for an acceleration at 160 Hz (initially), where the amplitude of the vibration ranged

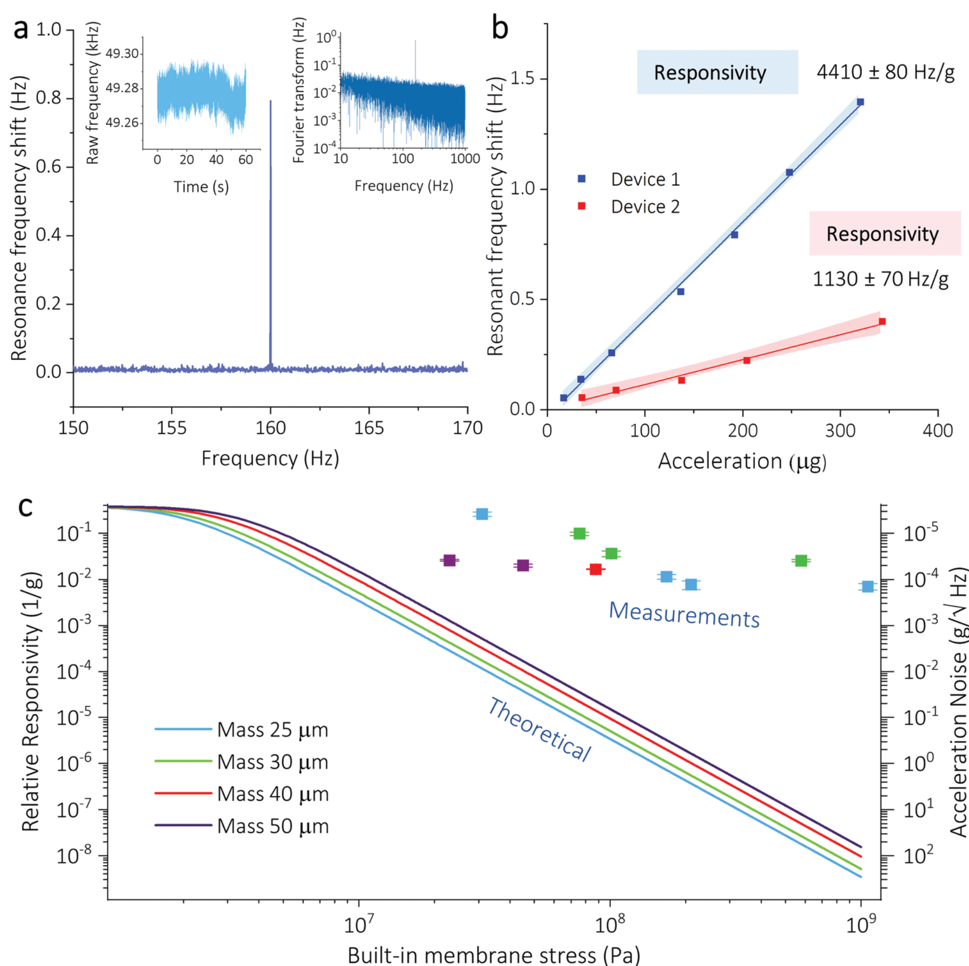

Figure 2. Experimental results and comparison with theory. a) Modulation of the resonance frequency of the system due to an externally applied sinusoidal acceleration at 160 Hz. This result is extracted from the fast Fourier transform (FFT) (inset right) of the captured frequency versus time signal (inset left) while the acceleration is applied. More details on the experimental setup can be found in Sections S5 and S6 in the Supporting Information. b) Magnitude of the resonance frequency modulation for different values of the externally applied acceleration, always a harmonic signal at 160 Hz. Two devices are exemplified here. Device 1 has a resonance frequency of 40 kHz and a Si proof mass with dimensions of $30 \times 30 \times 16.4$ µm^3. Device 2 has a resonance frequency of 168 kHz and a Si proof mass with dimensions of $25 \times 25 \times 16.4$ µm^3. A linear dependence between frequency modulation and acceleration is observed for both devices. The devices show responsivities of 4410 ± 80 and 1130 ± 70 Hz g^{-1}, respectively. The colored area around the data describes the 95% confidence band. c) (Plotted in squares) Experimentally extracted responsivities and acceleration noise density of ten different devices as a function of the estimated built-in stress. The noise density is extracted from the FFT of the frequency tracking data and then using the responsivity of each of the cases. These results are compared to the theoretical estimation (solid lines) from a model based on the inertial movement of the suspended mass. Strikingly, there is a difference of up to 6 orders of magnitude between both values.

© 2022 The Authors. Small published by Wiley-VCH GmbH

from 0.1 to 3 nm. We track the resonance frequency of the devices for 60 s (Figure 2a, left inset) and perform Fourier transform analysis to evidence a clear harmonic modulation of the frequency produced by the external load (Figure 2a, right inset). The relation between input load and frequency modulation is observed to be linear. In Figure 2b, the measurement results are shown for two different devices. Device 1 has a Si proof mass with dimensions of $30 \times 30 \times 16.4\ \mu m^3$ and a resonance frequency of 40 kHz, Device 2 has a Si proof mass with dimensions of $25 \times 25 \times 16.4\ \mu m^3$ and a resonance frequency of 168 kHz. The responsivity is the metric used to quantify the magnitude of the modulation produced by a certain acceleration (in 1/g units). We measured several devices, obtained their responsivity (Figure 2c) and compared them to the theoretical model validated through FEM simulations. A large discrepancy of up to six orders of magnitude can be seen between the predicted and measured responsivities, with the experimental results faring better than predicted. Furthermore, the experimental results, contrary to what the theory predicts, do not show any dependence of the responsivity with the suspended mass (see Section S7 and Figure S7 in the Supporting Information).

We then performed measurements at different acceleration frequencies to further investigate the mismatch between the expected and observed values. In these experiments, the amplitude of the external displacement load was fixed to 3 nm and we swept the frequency of the harmonic signal from 10 to 5 kHz (**Figure 3**a). The obtained results show that the response of the devices is nearly independent of the frequency at which the acceleration is applied, as opposed to a quadratic dependence expected if the modulations are proportional to the acceleration. When considering these results and the ones shown in Figure 2, it follows that the modulation of the resonance frequency is proportional to changes in the amplitude of the external load, rather than the acceleration. This also explains the discrepancy shown in Figure 2c between theory and experimental results, since the model only captures the inertial response and no other effects related to inhomogeneities in the shaking wave. The effect observed in our devices could be caused by a parasitic deformation of the substrate originated from a nonuniform transmission of the driving force. This effect can also be seen as a bending generated in the chip due to a small dephasing of the externally applied load, as schematized in Figure 3b. Such an effect would produce changes in the membrane stress and consequently would shift the resonance frequency. To test this hypothesis, we increased the stiffness of the chip by rigidly attaching it onto thicker substrates, thus reducing the bending of the chip during the experiments (Figure 3c). We used a thin (0.8 mm) and thick (2.8 mm) aluminum plate. In both cases, we repeated the experiment presented in Figure 2, with an external load produced at 160 Hz and changing the amplitude of vibration. Finally, we tested the chip using a commercial shaker (9110D, The Modal Shop), the sample was clamped directly to the calibration mounting adaptor (PVC-HTMNT01, stainless steel 1 cm thick) and larger vibrations could be probed. We found that increasing the bending stiffness of the chip leads to smaller modulations of the resonance frequency for the same external loads.

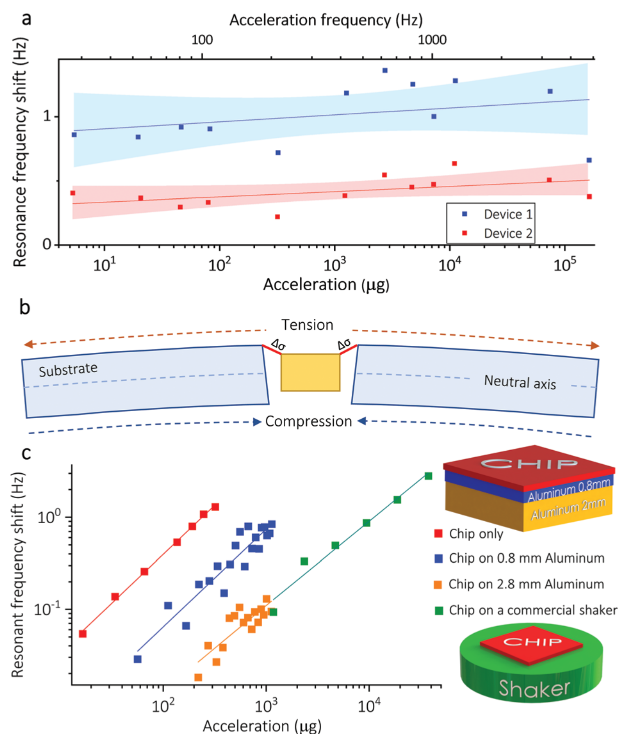

Figure 3. Vibration-induced bending effect. a) Resonance frequency shift as a function of externally applied acceleration. In this study, the vibration amplitude was kept constant, and the acceleration frequency ranged from 10 Hz up to 5 kHz. Linear fitting is depicted by solid lines and a 95% confidence band in colored areas. Changes in the modulation frequency have a very weak impact on the resonance frequency shift. This implies that most of the shift is caused not by an inertial force but by in-plane deformations in the top side of the wafer. b) The origin of this in-plane deformation is likely to be a small dephasing of the acoustic vibrations imposed on the chip while the vibration is loaded, as schematized. c) Experimentally obtained resonance frequency shifts as a function of acceleration while the modulation frequency was kept at 160 Hz, for three different clamping mechanisms of the same device. In this study, accelerations were produced by changing the vibration amplitude. The chip was first measured with the original substrate. To reduce the parasitic bending deformations, the chip was solidly bonded to different metallic plates. The 0.8 mm thick aluminum plate and the 2.8 mm thick plate reduced the measured responsivity in the devices. This latter chip was also probed at higher amplitudes by using a larger commercial shaker (9110D, The Modal Shop).

3. Discussion

The results shown in Figure 3 lead us to conclude that the observed modulation across our experiments is caused by a bending of our substrates/chips. We first explored other possibilities, more in line with the set of devices we have. One alternative hypothesis was that the effect is due to a weak van der Waals interfacial adhesion between the graphene and the SiO_2.[31] This could cause either a sliding of the graphene or a detachment of the graphene close to the anchor. In both cases, these effects would be proportional to the force applied by the acceleration on the graphene (via the central mass). From our measurements, we do not see any correlation between the force applied per perimeter length and the responsivity (see Section S8 and Figure S8 in the Supporting Information). This result

© 2022 The Authors. Small published by Wiley-VCH GmbH

suggests that the interfacial adhesion between graphene and SiO_2 is strong enough for the small amplitudes driven on the mass (≈5 nm). Consequently, the effect is likely to be caused by the aforementioned parasitic bending of the substrate and could be in principle seen in any resonator.

The reason why this effect is orders of magnitude higher than the inertial effect of the acceleration on the system is that the suspended masses of these devices are very small. Indeed, the effect presented in this paper is not visible in larger resonant accelerometers,[9] in which the signal is entirely dominated by the inertial response of the suspended mass.

As can be seen in Figure 2c, the experimental responsivities in our devices do not depend on the value of the Si proof mass (see also Section S7 and Figure S7 in the Supporting Information). We can even bring this to the limit and study devices with no suspended proof mass, just suspended graphene membranes. These extremely light devices respond to vibrations in a similar way as the ones with a suspended mass. A simple analysis tells us that, if our hypothesis of the frequency shifts being caused by membrane elongation due to chip bending is true, this would result in a modified responsivity (now defined as the relative shift over displacement) that would be inversely proportional to the membrane stress. When plotting the experimentally measured responsivities for 50 different devices, both with and without a suspended proof mass, this dependence emerges, in particular for the devices with proof mass (see **Figure 4**). The data of the devices without a suspended proof mass deviates further from the proportionality line compared to the other devices, and we believe this is due to an underestimation of the built-in stress in those cases. Since the membranes are so thin, any residues on top of the graphene (e.g., polymer residues originating in device fabrication) would amount to a very significant portion of the total mass, up to several times heavier than the graphene membrane. As the mass of the residues is very difficult to estimate, we assumed pristine membranes for the data points in Figure 4, which implies an underestimation of the actual built-in stress.

The modeling of how the vibration dephasing (or bending) originates in the interface between the piezo shaker and our devices is impossible to develop, given that we do not know the microscopic structure of said interface. However, our hypothesis that the substrate bending is the source of the change of stress in the graphene membranes and the associated signals was verified by FEM simulations (see Section S9 in the Supporting Information). The observed modulations in resonance frequency could be explained by a vertical dephasing of 0.1 pm between different sides of the membrane, which corresponds to a relative mismatch in the order of 10^{-5} when considering a typical vibration amplitude around 5 nm. We concluded that any small asymmetry in the piezo shaker or the back of the chip could generate this effect. Importantly, this may be one of the main reasons for some of the reported low-quality factor values of graphene devices, e.g., resonators over the past decade.[20,21,32] Essentially, every experiment where the actuation has been performed via a piezo shaker could be affected by this effect. If the vibration amplitude is large enough, the frequency will modulate at the same rate as the actuation itself and it could entail an artificially induced reduction of the quality factor.

Furthermore, even though this effect is indeed more visible on graphene membranes because they are extremely thin, we believe that it is present in every single NEMS and MEMS resonator (clamped on both ends) that is driven into motion using an external shaker. Evidently, it will not be evident in all cases, i.e., if the measured signal is dominated by the inertial response of a large proof mass, but it will be present. This supports, even more, the importance of clamping and actuation when performing studies on very high quality factor devices.

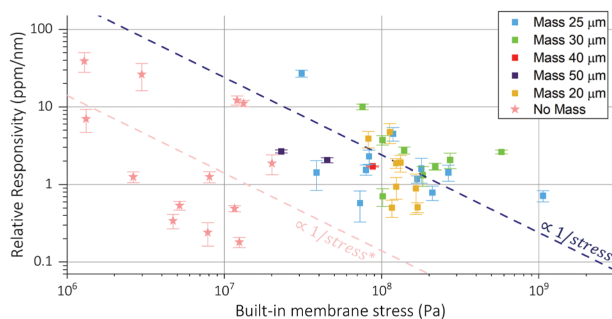

Figure 4. Responsivity comparison between devices with and without suspended mass. The relative responsivity is calculated for devices with suspended mass and graphene membranes. The responsivity is seen to be inversely proportional to the membrane stress. No difference is seen due to their attached mass (from $20 \times 20 \times 16.4$ to $50 \times 50 \times 16.4$ μm^3) or directly not having any proof mass. The membranes (without proof mass) measured have various diameters (30, 50, 75, 100, 200, and 300 μm). They have been represented with the same color to facilitate the plot comprehension. No differences are seen regarding the membrane diameter, being their stress the characterizing parameter. Importantly, the stress of the massless devices is sometimes underestimated since we have residues on the graphene surface, resulting in a larger total mass than we use for this calculation. The dispersion in responsivity for similar membrane stress in devices with attached mass could come from the non-uniformity in stress measured in the AFM.

4. Conclusion

In conclusion, our proposed graphene NEMS devices operating in resonant mode can be used as very high performing vibration sensors with an extremely small footprint. Even though the devices do not behave as originally predicted, they unveil a fundamental effect that might be present in every single MEMS and NEMS clamped flexural resonator. This effect will have a greater impact on devices with high quality factors as they are thinner and/or have very low stress.

5. Experimental Section

Fabrication Process: An SOI wafer was thermally oxidized to grow a 1.4 μm thick layer of SiO_2. The Si proof mass shape was patterned by optical lithography, reactive ion etching (RIE) and deep reactive ion etching (DRIE). Additionally, the buried oxide layer underneath the Si proof mass was exposed from the backside using optical lithography, RIE and DRIE. For the graphene membranes, commercially available CVD single-layer graphene films on copper (Graphenea, Spain) was used and double-layer graphene was prepared by vertically stacking two single layers of graphene on top of each other by using a wet transfer approach (PMMA-support transfer).[4,6] Afterwards, the double-layer graphene was transferred onto the prefabricated SOI device substrate using a

© 2022 The Authors. Small published by Wiley-VCH GmbH

conventional wet transfer process, and the transferred graphene was then patterned by optical lithography and O_2 plasma etching. To release the Si proof mass and suspend it on the graphene membrane, the box layer was sacrificially etched by RIE, followed by vapor HF etching. For more details on the fabrication, please refer to Section S3 (Supporting Information) and Fan et al.[4]

Characterization: The morphology of the devices during and after device fabrication were observed and characterized by optical microscopy and SEM imaging, respectively. The resonance frequency measurements of the graphene devices were carried out with a laser doppler vibrometer (LDV). The laser pointed at the device under test that was loaded over a piezoelectric element that converts a given input signal into vibrations in the -axis. The resonance frequency of the accelerometer was excited by that shaker. Simultaneously, a lower frequency signal was introduced to produce accelerations. The acceleration can be controlled by the amplitude and the frequency of that signal. The LDV signal was sent to a Lock-in amplifier to be read in displacement or velocity units. The Lock-in amplifier integrated a phase-locked loop (PLL), which tracked the resonance frequency over time. Later, a Fourier transform of the evolution of the resonance frequency allowed to obtain the shifts happening at a certain acceleration frequency. More details can be seen in Sections S5 and S6 in the Supporting Information.

Supporting Information

Supporting Information is available from the Wiley Online Library or from the author.

Acknowledgements

The authors thank Fredrik Forsberg, Stefan Wagner, and Cecilia Aronsson for discussions with device processing. This work was supported by the National Natural Science Foundation of China (Grant Nos. 62171037 and 62088101), the European Research Council through the Starting Grants M&M's (No. 277879) and InteGraDe (307311), the Swedish Research Council (GEMS, 2015–05112), the China Scholarship Council (CSC) through a scholarship grant, the FLAG-ERA project 2DNEMS funded by the Swedish Research Foundation (VR) (2019-03412) and the German Research Foundation (DFG) [LE 2441/11-1], the German Federal Ministry for Education and Research project NanoGraM (BMBF, 03XP0006C). Funding through the European Commission under the Horizon 2020 research program is gratefully acknowledged (Graphene Flagship, 881603). L.G.V. and D.M.G. thank the financial support from the Swiss National Science Foundation via grants PP00P2_170590 and CRSII5_189967.

Open access funding provided by Ecole Polytechnique Federale de Lausanne.

Conflict of Interest

The authors declare no conflict of interest.

Authors Contribution

D.M.G. and X.F. contributed equally to this work. D.M.G., L.G.V., X.F., and F.N. conceived and designed the experiments. A.D.S. and M.C.L. developed the graphene transfer method. X.F. fabricated the devices (substrate preparation, graphene transfer and patterning, and proof mass release). C.M.O. carried out the AFM characterization. D.M.G. and V.M. performed the vibration measurements. D.M.G. and L.G.V. developed the theoretical model, ran the finite element simulations, analyzed the experimental results and wrote the manuscript. X.F. and F.N. provided input in the paper. All authors discussed the results and commented on the manuscript.

Data Availability Statement

The data that support the findings of this study are available from the corresponding author upon reasonable request.

Keywords

graphene, laser doppler vibrometry, nano-electromechanical (NEMS), resonators, vibration

Received: March 22, 2022
Revised: May 9, 2022
Published online:

[1] J. Marek, presented at *2010 IEEE Solid-State Circuits Conference (ISSCC)*, San Francisco, USA **2010**, pp. 9–17.
[2] P. Zwahlen, A.-M. Nguyen, Y. Dong, F. Rudolf, M. Pastre, H. Schmid presented at *2010 IEEE 23rd Int. Conf. on Micro Electro Mechanical Systems (MEMS)*, Wanchai, Hong Kong, China, **2010**, pp 631–634.
[3] M. B. Del Rosario, S. J. Redmond, N. H. Lovell, *Sensors* **2015**, *15*, 18901.
[4] X. Fan, A. D. Smith, F. Forsberg, S. Wagner, S. Schröder, S. Akbari, A. C. Fischer, L. G. Villanueva, M. Östling, M. C. Lemme, F. Niklaus, *Microsystems & Nanoengineering* **2020**, *6*, http://doi.org/10.1038/s41378-019-0128-4.
[5] X. Fan, F. Forsberg, A. D. Smith, S. Schröder, S. Wagner, H. Rödjegård, A. C. Fischer, M. Östling, M. C. Lemme, F. Niklaus, *Nat. Electron.* **2019**, *2*, 394.
[6] X. Fan, F. Forsberg, A. D. Smith, S. Schröder, S. Wagner, M. Östling, M. C. Lemme, F. Niklaus, *Nano Lett.* **2019**, *19*, 6788.
[7] S. Schmid, M. L. Roukes, L. G. Villanueva, *Fundamentals of Nanomechanical Resonators*, 1st ed, Springer International Publishing, Switzerland **2016**, p. 175.
[8] S. Wang, X. Wei, Y. Zhao, Z. Jiang, Y. Shen, *Sens. Actuators, A* **2018**, *283*, 151.
[9] C. Zhao, M. Pandit, G. Sobreviela, P. Steinmann, A. Mustafazade, X. Zou, A. Seshia, *J. Microelectromech. Syst.* **2019**, *28*, 324.
[10] E. E. Moreira, B. Kuhlmann, J. Gaspar, L. A. Rocha, *Multidisciplinary Digital Publishing Institute Proceedings* **2018**, *2*, 1030.
[11] T. Mei, J. Lee, Y. Xu, P. Feng, *Micromachines* **2018**, *9*, 312.
[12] W. Niu, L. Fang, L. Xu, X. Li, R. Huo, D. Guo, Z. Qi, *J. Comput. Commun.* **2018**, *6*, 215.
[13] E. Borgia, *Comput. Commun.* **2014**, *54*, 1.
[14] M. C. Lemme, S. Wagner, K. H. Lee, X. G. Fan, G. J. Verbiest, S. Wittmann, S. Lukas, R. J. Dolleman, F. Niklaus, H. S. J. van der Zant, G. S. Duesberg, P. G. Steeneken, *Research* **2020**, *2020*, 1.
[15] C. Chen, J. Hone, *Proc. IEEE* **2013**, *101*, 1766.
[16] R. J. Dolleman, D. Davidovikj, S. J. Cartamil-Bueno, H. S. J. van der Zant, P. G. Steeneken, *Nano Lett.* **2016**, *16*, 568.
[17] M. Lee, D. Davidovikj, B. Sajadi, M. Siskins, F. Alijani, H. S. J. van der Zant, P. G. Steeneken, *Nano Lett.* **2019**, *19*, 5313.
[18] C. Lee, X. Wei, J. W. Kysar, J. Hone, *Science* **2008**, *321*, 385.
[19] S. A. Akbari, V. Ghafarinia, T. Larsen, M. M. Parmar, L. G. Villanueva, *Sci. Rep.-Uk* **2020**, 10. https://doi.org/10.1038/s41598-020-63562-y.
[20] J. S. Bunch, v. d. A. M. Zande, S. S. Verbridge, I. W. Frank, D. M. Tanenbaum, J. M. Parpia, H. G. Craighead, P. L. McEuen, *Science* **2007**, *315*, 490.
[21] v. d. A. M. Zande, R. A. Barton, J. S. Alden, C. S. Ruiz-Vargas, W. S. Whitney, P. H. Q. Pham, J. Park, J. M. Parpia, H. G. Craighead, P. L. McEuen, *Nano Lett.* **2010**, *10*, 4869.
[22] C. Chen, S. Rosenblatt, K. I. Bolotin, W. Kalb, P. Kim, I. Kymissis, H. L. Stormer, T. F. Heinz, J. Hone, *Nat. Nanotechnol.* **2009**, *4*, 861.

© 2022 The Authors. Small published by Wiley-VCH GmbH

[23] F. Ye, J. Lee, P. X. L. Feng, *Nano Lett.* **2018**, *18*, 1678.
[24] S. K. More, A. K. Naik, *J. Micromech. Microeng.* **2021**, 045015, https://doi.org/10.1088/1361-6439/abe20b.
[25] J. W. Kang, J. H. Lee, H. J. Hwang, K.-S. Kim, *Phys. Lett. A* **2012**, *376*, 3248.
[26] J. W. Kang, J. H. Park, G.-Y. Lee, K.-S. Kim, *J. Comput. Theor. Nanosci.* **2015**, *12*, 4186.
[27] K.-R. Byun, K.-S. Kim, H. J. Hwang, J. W. Kang, *J. Comput. Theor. Nanosci.* **2013**, *10*, 1886.
[28] W. Jie, F. Hu, X. Wang, S. Qin, presented at *Second Int. Conf. on Photonics and Optical Engineering (2016)*, Xi'an, China, **2017**, p. 102562E.
[29] F.-T. Shi, S.-C. Fan, C. Li, X.-B. Peng, *Sensors* **2018**, *18*, 2266.
[30] S. D. Senturia, *Microsystem Design*, Kluwer Academic Publishers, Boston **2001**, p. 689.
[31] W. Gao, P. H. Xiao, G. Henkelman, K. M. Liechti, R. Huang, *J. Phys. D: Appl. Phys.* **2014**, *47*, 255301.
[32] A. Eichler, J. Moser, J. Chaste, M. Zdrojek, I. Wilson-Rae, A. Bachtold, *Nat. Nanotechnol.* **2011**, *6*, 339.

© 2022 The Authors. Small published by Wiley-VCH GmbH